



# Tuning Time, Boosting Performance: Optimizing Crystallinity in Poly(Heptazine Imide) for Efficient Hydrogen Evolution

Luis F. G. Noleto<sup>1\*</sup>, Izadora F. Reis<sup>1</sup>, Ivo F. Teixeira<sup>1</sup>

<sup>1</sup>Universidade Federal de São Carlos (UFSCar) \*fernandoguimaraes621@gmail.com

## **Abstract**

A obtenção de nitretos de carbono altamente cristalinos é fundamental para aprimorar suas propriedades fotocatalíticas. Neste estudo, diferentes amostras de poli(heptazina imida) (PHI) foram sintetizadas variando-se o tempo de tratamento térmico (2, 3, 4, 6 e 8 h) e aplicadas na reação de evolução de hidrogênio. O material sintetizado por 4 h (Na-PHI-4) apresentou a melhor performance, com taxa de produção de 3151,9 μmol g<sup>-1</sup> h<sup>-1</sup> e eficiência quântica aparente de 3,09%. As análises de DRX, UV-Vis e fotoluminescência indicaram que esse material possui maior cristalinidade, melhor absorção de luz e menor recombinação de cargas. Tempos curtos de síntese resultaram em fases mistas e defeitos estruturais, enquanto tempos excessivos favoreceram degradação térmica e novos defeitos. Assim, o tempo de síntese mostra-se um fator crucial para controlar a cristalinidade e otimizar a atividade fotocatalítica de PHI.

Palavras-chave: Nitreto de carbono cristalino, Evolução fotocatalítica de hidrogênio, Poli(heptazina imida)

The synthesis of highly crystalline carbon nitrides is essential to enhance their photocatalytic properties. In this study, poly(heptazine imide) (PHI) samples were synthesized by varying the thermal treatment time (2, 3, 4, 6, and 8 h) and applied in the hydrogen evolution reaction. The material synthesized for 4 h (Na-PHI-4) showed the best performance, with a hydrogen production rate of 3151.9 µmol g<sup>-1</sup> h<sup>-1</sup> and an apparent quantum yield of 3.09%. XRD, UV-Vis, and photoluminescence analyses indicated that this material exhibited higher crystallinity, improved light absorption, and lower charge carrier recombination. Short synthesis times led to mixed phases and structural defects, while longer times caused slight thermal degradation and new defects. Therefore, synthesis time is a key factor in controlling crystallinity and optimizing the photocatalytic activity of PHI.

Keywords: Crystalline carbon nitride, Photocatalytic hydrogen evolution, Poly(heptazine imide)

## Introdution

Carbon nitrides (CNs) represent a class of robust and stable polymeric semiconductors that have garnered significant attention from the scientific community. Their basic structure is composed of naturally abundant elements such as carbon (C) and nitrogen (N), which can be arranged in various configurations to form a range of allotropes. A notable example is Polymeric carbon nitrides (PCNs) are composed of layered polymeric structures formed by covalently bonded heptazine units. However, due to their typically low crystallinity and structural disorder, these materials suffer from poor reproducibility in synthesis and limited photocatalytic performance, mainly because of enhanced charge carrier recombination caused by abundant structural defects and trap states [1].

Strategies to enhance crystallinity and reduce structural defects in carbon nitrides (CNs) include the use of alternative synthesis methods, such as the molten salt approach. Poly(triazine imide) (PTI) and poly(heptazine imide) (PHI), for example, are carbon nitride allotropes obtained through this method that stand out due to their highly crystalline and well-defined structures <sup>[2]</sup>. These materials have already been applied in various fields, such

as energy conversion and organic synthesis [3, 4]. Additionally, several studies have been conducted to explore the increase in crystallinity and its influence on the photocatalytic properties of PHI, highlighting its potential in advanced photocatalytic processes. These investigations include variations in synthesis temperature [5], the use of different precursors and salt combinations [6], as well as changes in thermal treatment duration, all aimed at tuning the structural and electronic properties of PHI to enhance its photocatalytic performance. For example, Lin et al. prepared CN at different synthesis temperatures and found that the material obtained from a precursor pre-heated at 550 °C exhibited the highest crystallinity and photocatalytic activity for hydrogen production, achieving an apparent quantum yield (AQY) of 6.8% at 420 nm using methanol as a sacrificial agent [5].

In this work, we investigated the influence of the thermal treatment duration used during the synthesis of Na-PHI on its physicochemical properties, with an emphasis on the degree of structural organization of the obtained materials. In parallel, we evaluated the photocatalytic activity of these materials in hydrogen evolution reactions (H<sub>2</sub>).



## Experimental

Synthesis of Na-PHI:

Na-PHI samples were synthesized for the thermal condensation method, using Melamine assisted by sodium chloride (NaCl) <sup>[4]</sup>. In this procedure, melamine (1 g) and NaCl (10 g) were ground to a complete mixture. The solid was transferred into an alumina crucible and heated (2.3 °C.min<sup>-1</sup>) under nitrogen flow (80 L.min<sup>-1</sup>) for 2, 3, 4, 6 and 8 h. Samples were designated according to the duration of the thermal treatment: Na-PHI-X (where *X*: 2, 3, 4, 6, or 8).

To comprehensively evaluate the structural and optical features of the synthesized materials, a combination of characterization techniques was employed, including X-ray diffraction (XRD), attenuated total reflectance Fourier-transform infrared spectroscopy (ATR-FTIR), UV–Vis absorption spectroscopy, steady-state photoluminescence (PL), and time-resolved photoluminescence (Tr-PL).

## Photocatalytic reaction:

The photocatalytic tests were carried out in a sealed reactor using degassed deionized water (DI) under an Ar atmosphere to prevent the presence of O<sub>2</sub>, which could interfere with the water reduction reaction. A suspension containing 30 mL of DI, 50 mg of solid catalyst, and 10% triethanolamine (TEOA) was exposed to irradiation from a 50 W LED lamp at 410 nm. The Pt cocatalyst was incorporated *in situ* into the PHI framework through photodeposition, using a 3% aqueous solution of K<sub>2</sub>PtCl<sub>4</sub> as a precursor. The initial hour of irradiation, dedicated to Pt photodeposition, was not considered for hydrogen detection. The amount of hydrogen produced was determined by monitoring the pressure inside the reactor with a P-30 digital pressure sensor from Wika.

## Results and Discussion

Characterization of Materials:

In order to investigate the degree of crystallinity or any influence promoted by the different heat treatment durations on the Na-PHI structure, X-ray diffraction (XRD) analysis was performed. As shown in **Figure 1a**, heat treatment duration is a key factor for obtaining more crystalline Na-PHI structures. The increase in the intensity of the reflection peaks can be directly related to the degree of polymerization of the heptazine units in-plane to form the longest 2D structures and to the stacking of the layers. Similar characteristic peaks at 8.1°, 14.3°, and 27.3° were found in all samples and can be attributed to (100), (110), and (002) planes, respectively, according to a reported layered triclinic structure of PHI (Cell parameters:  $a = b \neq c$ ,  $\alpha = \beta \neq \gamma$ ) [2.7]. The Na-PHI samples treated for 2 and 3 h also showed an



additional signal at 12.8° related to the (100) plane of the polymeric carbon nitride (PCN) phase. This signal disappears completely with increasing polymerization time, confirming the transition to the crystalline poly(heptazine imide) (PHI) phase [8]. On the other hand, the signal near 8.1°, which relies on the formation of PHI structures, increases in intensity, again confirming the formation of more crystalline structures (Na-PHI-2 < Na-PHI-3 < Na-PHI-4), see in **Figure 1b**. However, a slight decrease in this signal is observed after 4 hours of thermal treatment. This may be an indication that the structure is undergoing some form of degradation or alteration due to prolonged exposure to thermal treatment.

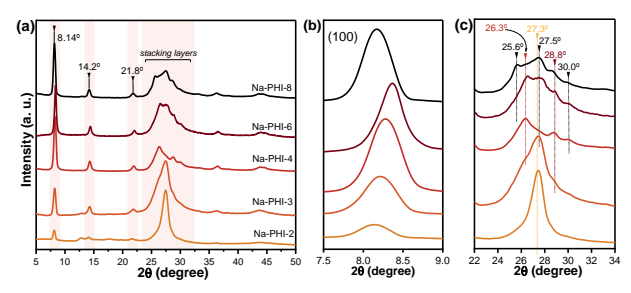


**Figure 1.** (a) XRD patterns for Na-PHI samples treated at different times. Magnified region between (b) 7.5°–9.0° and (c) 22°–34°.

Interestingly, the diffraction signal attributed to the (002) crystallographic plane of the Na-PHI samples shows small differences in their peak profiles, as shown in Figure 1c. Na-PHI-2 is similar and exhibits a single peak located at 27.3°, while Na-PHI-3 shows a slight shift to higher values and a widening of the signal. This small shift can be attributed to stronger interactions between the layers, which in turn are becoming more extensive due to more favorable reaction conditions for polymerization. More importantly, for Na-PHI-4, Na-PHI-6, and Na-PHI-8, new diffraction peaks at 25.6°, 26.3°, 27.3°, 27.5°, 28.8°, and 30.0° are gradually emerging, likely due to the emergence of new planes with different directions and different stacking patterns between the layers [9]. In general, the adjustment in the stacking of layers in carbon nitride structures can directly affect the electron coupling between layers, which interferes with the material's light absorption process [10]. As a result, light absorption can be extended into the visible region, as will be discussed later.

The structural information of the samples was further analyzed by attenuated total reflectance Fourier transform infrared (ATR-FTIR) spectroscopy, as presented in **Figure 2a**. The broad absorption band at 3650–2761 cm<sup>-1</sup> suggests the presence of the surface hydroxyl groups, surface adsorbed water, and terminal amino groups (**Figure 2b**). It is easily observed that the Na-PHI-2 exhibits a vibration



band associated with C-N groups that are more defined and well separated from the other bands attributed to O-H and C-H groups [11]. This behavior is related to the predominance amino-type defects, which of progressively eliminated as the thermal treatment is extended. In the other Na-PHI spectra (3, 4, 6, and 8), the three bands become practically indistinguishable and are shifted to higher wavenumbers, corresponding to the O-H vibration region. Furthermore, the stretching mode of the cyanamide moiety (associated with defect groups formed by terminal cyanamides) corresponds to the band at 2173 cm<sup>-1</sup> [11]. The intensity of this band decreases as the heat treatment time increases from 2 to 4 h, indicating a higher degree of organization within the 2D structure of PHI. However, when the synthesis time exceeds 4 h, the intensity of this band increases, which could be attributed to increased disorder and the formation of additional defect groups, possibly formed by heptazine ring decomposition. The peaks from 1626, 1451, 1393, 1310, and 1205 cm<sup>-1</sup> are attributed to the expansion vibration of the heterocyclic aromatic C<sub>6</sub>N<sub>7</sub> heptazine. The peak at 1573 cm<sup>-1</sup> is attributed to stretching vibrations of the C-N bonds (Figure 2c) [12]. The bands at 1065 and 985 cm<sup>-1</sup> are related to the symmetric and asymmetric vibrations of NC<sub>2</sub> bonds in metal-NC<sub>2</sub> groups, respectively [13]. Finally, the bands at 800 cm<sup>-1</sup> and 887 cm<sup>-</sup> correspond to the presence of s-triazine in the poly(heptazine imide) structure. This bending is caused by the vibration of the tri-s-triazine (heptazine) ring (shown in the right panel of Figure 2c).

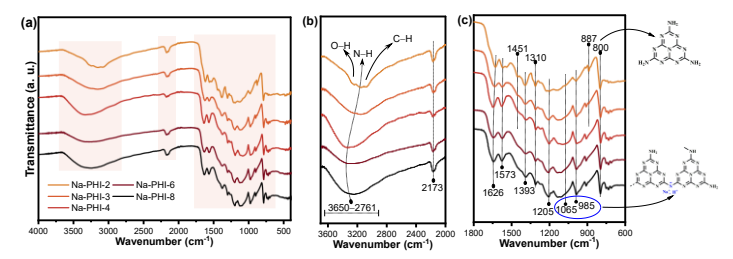


**Figure 2.** (a) FTIR spectra for Na-PHI samples treated at different times. Amplified region between (b)  $3700-2000 \text{ cm}^{-1}$  and (c)  $1800-600 \text{ cm}^{-1}$ .

The optical absorption properties of the samples were investigated by UV–Visible Diffuse Reflectance Spectroscopy (UV–Vis DRS). According to **Figure 3a**, the visible light absorption intensities of Na-PHI (3, 4, 6, and 8) are significantly higher than those of Na-PHI-2, which can be attributed to the increase in the crystallinity and higher polymerization degree. Na-PHI exhibits an intrinsic absorption band primarily originating from the  $\pi \rightarrow \pi^*$  transition of sp²-hybridized carbon and nitrogen within the tri-s-triazine skeletons. During this transition, which is allowed for perfectly symmetric and planar heptazine units, excited-state electrons are promoted from the highest



occupied molecular orbital ( $\pi$  HOMO) to the lowest unoccupied molecular orbital ( $\pi$ \* LUMO), constituting the fundamental transition [14]. This process gives rise to the absorption boundary at approximately 460 nm. Conversely, a second transition, the  $n\rightarrow\pi^*$  transition, can be observed in certain carbon nitride-based materials. This transition is typically restricted to the symmetrical and coplanar structure of pristine CN, and it often requires structural distortions or the incorporation of  $\pi$ -deficient conjugated electron monomers to become prominent [8, 14, 15]. A step-like Urbach tail attributed to the  $n \rightarrow \pi^*$  transition is prominently observed in the region from 450 to 700 nm for Na-PHI-6 and Na-PHI-8. This feature can be ascribed to the increasing layers condensation and layers distortion resulting from the extended treatment time, which is consistent with the appearance of new planes and different layers in the Na-PHI-6 and Na-PHI-8 samples, as previously discussed in the XRD results. In this context, it was determined that the ideal thermal treatment time to achieve a highly crystalline and ordered poly(heptazine imide) synthesis, without significant structural disturbances, is 4 h. This is evidenced by the Na-PHI-4 spectrum, which shows a more consistent absorption profile and a baseline without major oscillations.

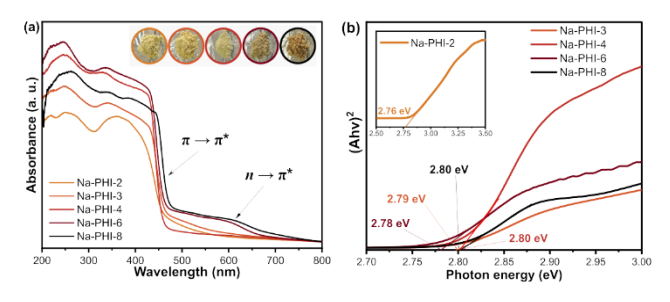


**Figure 3.** (a) UV-Vis absorption spectra and (b-c) band gap energy for Na-PHI synthesized at different heat treatment times.

The photophysical properties of photogenerated carriers Na-PHI samples were investigated photoluminescence (PL) spectroscopy. As is well establlished, reducing the recombination rates photogenerated electron-hole pairs is crucial for the enhancement of photocatalyst performance. In this case, the electron-hole pair separation efficiency of the samples can be detected by PL steady-state, since the stronger PL peak intensity generally represents a higher rate of electron and hole recombination [16]. In general, the intensity of the PL peak for materials like carbon nitrides can be reduced by different factors. For instance, extending the  $\pi$ -conjugated system by connecting additional heptazine units results in an expanded  $\pi$ -state and stronger orbital overlap [5]. Additionally, reducing the number of defects within the structure also plays a crucial role in this behavior. As shown in Figure 4a, all Na-PHI samples exhibit peaks located at 460 nm, attributed to intra-band transitions between the



conduction and valence bands. In more detail, the PL emission peaks of the Na-PHI samples (4, 6, and 8) exhibit significantly lower intensity compared Na-PHI-2 and Na-PHI-3, indicating greater suppression of the recombination of photogenerated charge carriers. These results are consistent with the structural characterization performed by XRD, which demonstrated an increase in the condensation rate of heptazine units due to the longer thermal treatment time of Na-PHI, implying a marked increase in the crystallinity of these materials.

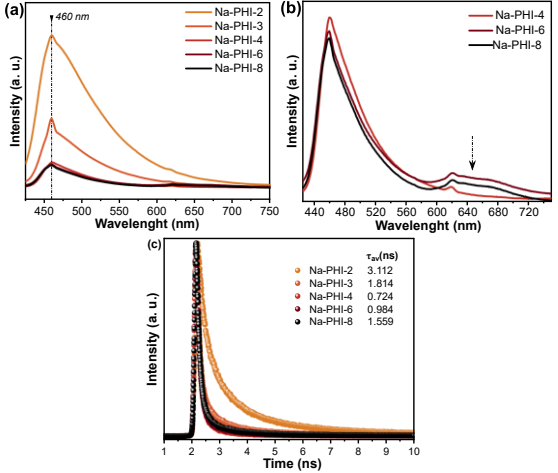


**Figure 4.** PL spectra (a, b) and Tr-PL decay curves (c) for Na-PHI samples treated at different calcination times.

No significant variations in the wavelength of the maximum emission peaks of the materials were observed; however, the appearance of a band above 600 nm was noted, especially for the Na-PHI samples treated for 6, and 8 h, as shown in **Figure 4b**. This behavior was also reported in the UV-vis spectra. Defects could lead to emissions at higher wavelengths, resulting in the observed tail. Here, transitions from lone pair states of nitrogen atoms in the s-triazine moiety, from amino groups, from NH bridging moieties, or possibly from graphitic regions give rise to the PL emission signals.

The separation of photoinduced charge carriers was evaluated based on the lifetimes obtained by time-resolved photoluminescence (Tr-PL) spectroscopy, on nanosecond (ns) scale, as shown in Figure 4c. The carrier lifetimes of the samples were obtained by fitting the data of tr-PL spectra using a multi-exponential decay model, and the average lifetime  $(\tau_{av})$  of the charge carriers was calculated by the following equation:  $\tau av = (A_1\tau_1^2 +$  $A_2\tau_2^2$  /( $A_1\tau_1 + A_1\tau_2$ ) [17]. The lifetimes  $\tau_1$  and  $\tau_2$  correspond to the fast and slow fluorescence decay components, respectively. The shorter lifetime component  $(\tau_1)$  is attributed to non-radiative recombination processes, which are proposed to originate from ultrafast electron transfer events occurring immediately after excitation. These processes effectively divert the excited carriers away from



the emissive state, thereby quenching photoluminescence. In contrast, the longer lifetime component ( $\tau_2$ ) corresponds to radiative recombination, where the excited carriers relax through photon emission <sup>[18]</sup>. Compared to the samples Na-PHI-2 (3.112 ns), Na-PHI-3 (1.814 ns), Na-PHI-6 (0.984 ns), and Na-PHI-8 (1.559 ns), the Na-PHI-4 sample exhibits the lowest average fluorescence lifetime ( $\tau_{av}$ ), of 0.724 ns (see in **Table 1**). This reduced  $\tau_{av}$  value suggests a more effective suppression of non-radiative recombination processes, thereby enhancing charge transfer within the material, which is highly beneficial for photocatalytic reactions due to its higher degree of crystallinity and structural organization.

**Table 1.** PL lifetime calculated from time-resolved PL spectra decay curve based on multi-exponential decay.

Sample	τ <sub>1</sub> (ns)	τ <sub>2</sub> (ns)	τ <sub>3</sub> (ns)	τ <sub>av</sub> (ns)
PCN	13.92	3.141	0.771	4.107
Na-PHI-2	10.61	1.810	0.326	3.112
Na-PHI-3	7.09	1.026	0.0894	1.814
Na-PHI-4	5.08	0.559	0.0799	0.724
Na-PHI-6	5.23	0.690	0.0754	0.984
Na-PHI-8	7.56	0.937	0.0932	1.559

Additionally, PCN was used as a reference, since this class of carbon nitride exhibits low crystallinity, along with a higher density of structural defects and recombination centers, which limit charge transfer. It is observed that the values of  $\tau_1$ ,  $\tau_2$ ,  $\tau_3$ , and  $\tau_{av}$  are higher for this sample (see in **Table 1**); however, they are comparable to those observed for the Na-PHI material thermally treated for 2 h, corroborating the XRD results. This similarity may indicate that these two samples contain a mixed PCN/PHI phase, undergoing a transition toward the formation of the pure poly(heptazine imide) phase.

## Photocatalytic Hydrogen Evolution Reaction (HER):

The performance of the different Na-PHI samples was evaluated in the photocatalytic production of H<sub>2</sub>. For this, was used an aqueous solution of triethanolamine (10 wt%) and Pt (3 wt%) as a co-catalyst, which was deposited on the surface of the materials through the photodeposition method using K<sub>2</sub>PtCl<sub>4</sub> as a precursor. As shown in **Figure 5**, the hydrogen evolution rate (HER) gradually increases with the increase in the thermal treatment time of Na-PHI-2 to Na-PHI-4. This increase may be related to improvements in the structural and optical properties of Na-PHI, such as enhanced structural ordering, the extension of heptazine units, higher energy absorption, and the suppression of charge carrier recombination. Comparing the different photocatalysts, Na-PHI-4 shows the highest H<sub>2</sub> evolution



rate of 3151.9  $\mu$ mol g<sup>-1</sup> h<sup>-1</sup>, while Na-PHI treated at 2 and 3 h produced only 1846.6 and 2717.1  $\mu$ mol g<sup>-1</sup> h<sup>-1</sup>, respectively. However, it is possible that a decrease in evolution rates with the extension of treatment time from 4 h to 6 h (2900  $\mu$ mol g<sup>-1</sup> h<sup>-1</sup>) and 8 h (2776.85  $\mu$ mol g<sup>-1</sup> h<sup>-1</sup>), may be attributed to the formation of structural defects. In addition, the apparent quantum yield (AQY%) for these reactions followed the same trend, with values of 2.24, 2.64, 3.09, 2.93 and 2.70% for Na-PHI-2, Na-PHI-3, Na-PHI-4, Na-PHI-6 and Na-PHI-8, respectively.

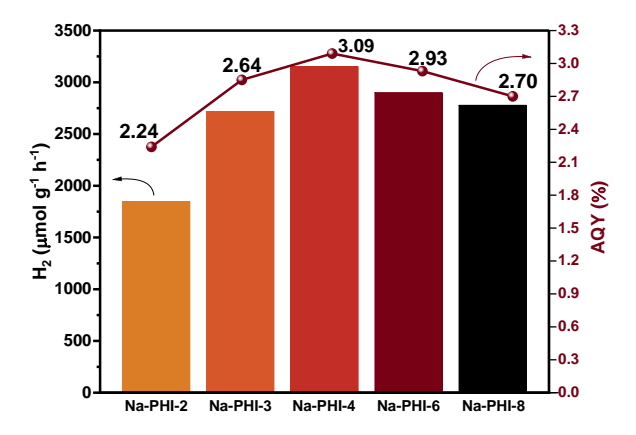


**Figure 5.** HER performance for Na-PHI catalysts.

According to the structural and optoelectronic characterizations, a consistent trend is observed in the formation of the extended PHI structure, which is directly associated with the thermal treatment time of the precursors and significantly impacts the hydrogen evolution results. Initially, at shorter time 2 h, the formation of longer PHI chains is partially hindered by the presence of the polymeric phase (PCN) in the mixture. These findings indicate a material with a mixed and defect-rich structure, which acts as recombination centers and impairs photocatalytic performance (1846.6 µmol g<sup>-1</sup> h<sup>-1</sup>). With the increase in treatment time to 3 h, the PCN fraction present in the mixture is almost entirely converted into PHI, thanks to the action of the structure-directing salt (NaCl), making the photocatalyst more efficient in the hydrogen evolution reaction (2717.1 µmol g<sup>-1</sup> h<sup>-1</sup>). After 4 h of thermal treatment, considered here the optimal synthesis time, a PHI structure with more extended layers, a higher degree of organization, and a lower defect density is observed. As a result, this structure becomes more efficient at promoting photocatalytic H<sub>2</sub> evolution, reaching a production rate of 3151.9 µmol g<sup>-1</sup> h<sup>-1</sup>. However, longer synthesis times, such as 6 and 8 h, lead to structural distortion and even degradation, which favor the formation of defects that impair photocatalytic performance. This is reflected in a gradual decrease in H<sub>2</sub> production rates, with values of 2900 μmol g<sup>-1</sup> h<sup>-1</sup> for Na-PHI-6 and 2776.85 μmol g<sup>-1</sup> h<sup>-1</sup> for Na-PHI-8.



## Conclusions

The photocatalytic performance of Na-PHI is strongly influenced by the duration of the thermal treatment during synthesis. Na-PHI-4 proved to be the ideal catalyst for the hydrogen evolution reaction, corresponding to a well-ordered PHI structure with few defects. Shorter or longer treatments led to incomplete conversion or structural degradation, respectively. These results emphasize the essential role of synthesis time in tuning the properties of PHI.

## Acknowledges

The authors acknowledges the financial support by the Brazilian funding agencies FINEP, CAPES, CNPq (423196/2018-9, 403064/2021-0 and 405752/2022-9) and FAPESP (2020/14741-6, 2021/13271-9, 2021/14006-7, 2021/12394-0, 2022/14652-9, 2021/13271-9, 2021/14006-7 and 2022/04748-9).

## References

- [1] F. Fina, S. K. Callear, G. M. Carins, J. T. Irvine, *Chemistry of Materials* **2015**, 27, 2612; Y. Wang, S. Z. F. Phua, G. Dong, X. Liu, B. He, Q. Zhai, Y. Li, C. Zheng, H. Quan, Z. Li, *Chem* **2019**, 5, 2775.
- [2] Z. Chen, A. Savateev, S. Pronkin, V. Papaefthimiou, C. Wolff, M. G. Willinger, E. Willinger, D. Neher, M. Antonietti, D. Dontsova, *Advanced Materials* **2017**, 29, 1700555.
- [3] M. A. R. da Silva, I. F. Silva, Q. Xue, B. T. W. Lo, N. V. Tarakina, B. N. Nunes, P. Adler, S. K. Sahoo, D. W. Bahnemann, N. López-Salas, A. Savateev, C. Ribeiro, T. D. Kühne, M. Antonietti, I. F. Teixeira, *Applied Catalysis B: Environmental* **2022**, 304, 120965; M. A. R. da Silva, N. V. Tarakina, J. B. G. Filho, C. S. Cunha, G. F. S. R. Rocha, G. A. A. Diab, R. A. Ando, O. Savateev, I. Agirrezabal-Telleria, I. F. Silva, S. Stolfi, P. Ghigna, M. Fagnoni, D. Ravelli, P. Torelli, L. Braglia, I. F. Teixeira, *Advanced Materials* **2023**, 35, 2304152.
- [4] M. A. R. da Silva, G. F. S. R. Rocha, G. A. A. Diab, C. S. Cunha, V. G. S. Pastana, I. F. Teixeira, *Chemical Engineering Journal* **2023**, 460, 141068.
- [5] L. Lin, W. Ren, C. Wang, A. M. Asiri, J. Zhang, X. Wang, *Applied Catalysis B: Environmental* 2018, 231, 234.
  [6] D. Burmeister, J. Müller, J. Plaickner, Z. Kochovski, E. J. W. List-Kratochvil, M. J. Bojdys, *Chemistry A European Journal* 2022, 28, e202200705.
- [7] H. Schlomberg, J. Kröger, G. Savasci, M. W. Terban, S. Bette, I. Moudrakovski, V. Duppel, F. Podjaski, R. Siegel, J. Senker, R. E. Dinnebier, C. Ochsenfeld, B. V. Lotsch, *Chemistry of Materials* **2019**, 31, 7478.
- [8] W. Wang, Z. Shu, J. Zhou, H. Tang, T. Li, D. Meng, ACS Applied Materials & Interfaces 2022, 14, 41131.
- [9] Z. Pan, M. Zhao, H. Zhuzhang, G. Zhang, M. Anpo, X. Wang, *ACS Catalysis* **2021**, 11, 13463; G. Zhang,





- Y. Xu, J. Zhu, Y. Li, C. He, X. Ren, P. Zhang, H. Mi, *Applied Catalysis B: Environmental* **2023**, 338, 123049.
- [10] H. Zhang, A. Yu, The Journal of Physical Chemistry C 2014, 118, 11628; F. Wu, Y. Liu, G. Yu, D. Shen, Y. Wang, E. Kan, The Journal of Physical Chemistry Letters 2012, 3, 3330.
- [11] L. Jiang, J. Yang, X. Yuan, J. Guo, J. Liang, W. Tang, Y. Chen, X. Li, H. Wang, W. Chu, *Advances in Colloid and Interface Science* **2021**, 296, 102523.
- [12] X. Yuan, K. Luo, K. Zhang, J. He, Y. Zhao, D. Yu, *The Journal of Physical Chemistry A* **2016**, 120, 7427; A. Savateev, D. Dontsova, B. Kurpil, M. Antonietti, *Journal of Catalysis* **2017**, 350, 203.
- [13] K. Akaike, A. Hosokai, H. Nagashima, Q. Wei, T. Hosokai, *Physical Chemistry Chemical Physics* **2022**, 24, 17504.
- [14] J. Lin, W. Tian, H. Zhang, H. Sun, S. Wang, Accounts of Chemical Research 2024, 57, 2303.
- [15] G. Zhang, A. Savateev, Y. Zhao, L. Li, M. Antonietti, *Journal of Materials Chemistry A* **2017**, 5, 12723.
- [16] Y. Zhang, N. Cao, X. Liu, F. He, B. Zheng, C. Zhao, Y. Wang, *Science China Materials* **2023**, 66, 2274; T. R. Stara, S. Y. Kuchmiy, *Theoretical and Experimental Chemistry* **2022**, 58, 240.
- [17] E. Mitchell, A. Law, R. Godin, *Journal of Photochemistry and Photobiology C: Photochemistry Reviews* **2021**, 49, 100453.
- [18] Q. Li, R. Yang, Z. Ma, S. Liu, D. Li, D. Tian, D. Jiang, *ChemSusChem* **2025**, 18, e202402000.